Journal of Biomolecular NMR **29:** 175–185, 2004.

Binding ability of a HHP-tagged protein towards Ni^{2+} studied by paramagnetic NMR relaxation: The possibility of obtaining long-range structure information

Malene Ringkjøbing Jensen[a], Conni Lauritzen[b], Søren Weis Dahl[b], John Pedersen[b] & Jens J. Led[a,*]

[a]*Department of Chemistry, University of Copenhagen, The H.C. Ørsted Institute, Universitetsparken 5, DK-2100 Copenhagen Ø, Denmark;* [b]*Unizyme Laboratories A/S, Dr. Neergaardsvej 17, DK-2970 Hørsholm, Denmark*

Received 15 October 2003; Accepted 2 January 2004

Key words: E. coli thioredoxin, metal binding tag, nickel, paramagnetic NMR, protein structure

Abstract

The binding ability of a protein with a metal binding tag towards Ni^{2+} was investigated by longitudinal paramagnetic NMR relaxation, and the possibility of obtaining long-range structure information from the paramagnetic relaxation was explored. A protein with a well-defined solution structure (*Escherichia coli* thioredoxin) was used as the model system, and the peptide His-His-Pro (HHP) fused to the N-terminus of the protein was used as the metal binding tag. It was found that the tag forms a stable dimer complex with the paramagnetic Ni^{2+} ion, where each metal ion binds two HHP-tagged protein molecules. However, it was also found that additional sites in the protein compete with the HHP-tag for the binding of the metal ion. These binding sites were identified as the side chain carboxylate groups of the aspartic and glutamic acid residues. Yet, the carboxylate groups bind the Ni^{2+} ions considerably weaker than the HHP-tag, and only protons spatially close to the carboxylate sites are affected by the Ni^{2+} ions bound to these groups. As for the protons that are unaffected by the carboxylate-bound Ni^{2+} ions, it was found that the long-range distances derived from the paramagnetic relaxation enhancements are in good agreement with the solution structure of thioredoxin. Specifically, the obtained long-range paramagnetic distance constraints revealed that the dimer complex is asymmetric with different orientations of the two protein molecules relative to the Ni^{2+} ion.

Abbreviations: NOE – nuclear Overhauser enhancement; *E. coli* – *Escherichia coli*; Trx – thioredoxin; IMAC – immobilized metal ion affinity chromatography; HT-DPPI – Polyhistidine-tagged dipeptidyl peptidase I; IPTG – isopropyl-1-thio–galactopyranoside; IR – inversion recovery; RMSD – root mean square deviation.

Introduction

The NMR method used for determining the solution structures of proteins relies primarily on short ($\leq$ 5 Å) inter-proton distance constraints derived from dipole-dipole interactions between protons close in space (Wüthrich, 1986; Wüthrich, 1994). Experimentally, these constraints are obtained from the nuclear Overhauser enhancements (NOEs). A weakness of this approach is the limited number of NOE constraints between residues far apart in the sequence. These constraints are essential for the determination of the tertiary fold of the protein, and a limited number may result in a poor determination of the tertiary structure. This holds, in particular, for larger proteins where relatively few long-range NOE constraints can be obtained.

The use of residual nuclear dipole couplings, observed in proteins that are partly oriented in the magnetic field (Tolman et al., 1995; Tjandra et al., 1997; Tjandra and Bax, 1997), has alleviated this long-range

*To whom correspondence should be addressed. E-mail: led@kiku.dk

order problem, as clearly demonstrated in recent years. However, the dipole interactions between the protons and the unpaired electrons of a paramagnetic metal ion located in the protein provide another source of long-range structure information. These interactions are more than 10^5 times stronger than the corresponding proton-proton interactions and can, therefore, affect nuclei located more than 20 Å from the metal ion.

The long-range electron-nuclear structure information can be obtained from the paramagnetic relaxation enhancements and the pseudo contact shifts of the nuclei in proteins containing a paramagnetic metal ion. Previously, structure constraints derived from these parameters have been used successfully in the refinement of the structures of native metalloproteins (Bertini et al., 1996) and metal complexes of nucleic acids (Tu and Gochin, 1999; Gochin, 2000). However, only a few studies have been reported where the paramagnetic constraints were obtained from metal ions artificially incorporated in proteins (Gaponenko et al., 2000, 2002; Donaldson et al., 2001; Mal et al., 2002).

Here, we investigate the applicability of a new metal binding tag consisting of two histidine residues and one proline residue (HHP). Primarily, we focus on the binding ability of a HHP-tagged protein towards Ni^{2+}, and the feasibility of obtaining long-range structure information from a Ni^{2+} ion bound to the tag. *A priori*, the HHP-tag seems attractive since it resembles the well-known his-tag used in protein purification. Furthermore, it is easily incorporated in most proteins that can be produced biotechnologically. Also, the proline linker and the short length make the tag relatively rigid, ensuring a well-defined position of the metal ion with respect to the protein. However, the ideal metal binding tag must also fulfill a series of other conditions. First, the metal binding must be specific with only one metal ion in a well-defined complex. Second, the binding constant should be sufficiently large to prevent severe competition from other potential binding sites in the protein. Last, but not least, the metal binding tag must not affect the structure of the protein.

The longitudinal paramagnetic relaxation of the amide protons was used to investigate both the Ni^{2+} binding ability of a HHP-tagged protein, and the long-range distance information that can be obtained from the nuclear paramagnetic relaxation. The applied model protein was the oxidized form of ^{15}N-labeled *Escherichia coli* (*E. coli*) thioredoxin (Trx). Trx is a 11.7 kD protein containing 108 amino acids. It is a multifunctional protein that participates in many different redox reactions through the reversible oxidation of two free thiol groups to a disulfide bridge at the active site (Holmgren, 1985). Highly accurate solution structures of both the oxidized and the reduced form of *E. coli* Trx have been determined (Jeng et al., 1994; Dyson et al., 1990), making the protein suitable for the investigations here. In the following, the residues HHP in the tagged protein (HHP-Trx) are numbered from -2 to 0 to retain the residue numbering from the untagged protein.

Theory

The longitudinal relaxation rates of the ligand nuclei in a paramagnetic metal complex are given by

$$R_1 = R_1^{\mathrm{dia}} + R_{1\mathrm{p}}. \tag{1}$$

Here, R_1^{dia} is the diamagnetic contribution as observed in a corresponding diamagnetic complex, while $R_{1\mathrm{p}}$ is the paramagnetic relaxation enhancement caused by the interaction of the nuclei with the unpaired electrons. The $R_{1\mathrm{p}}$ rate includes three contributions, the dipolar relaxation, the Curie spin relaxation, and the Fermi contact relaxation. The Fermi contact relaxation is caused by the modulation of the electron-nucleus scalar coupling. Since this coupling propagates through no more than five to six bonds, it is important only for nuclei relatively close to the paramagnetic center. The Curie spin relaxation stems from the dipolar interaction of the nuclear spin with the magnetic moment of the thermally averaged electron spin (Gueron, 1975; Vega and Fiat, 1976). For small proteins, like thioredoxin ($M_{\mathrm{w}} \approx 12$ kD), the Curie spin relaxation is significant only for the transverse relaxation, while the longitudinal relaxation remains unaffected by this mechanism. Thus, $R_{1\mathrm{p}}$ is given entirely by the dipolar interaction between the nuclear spin and the unpaired electron spin.

If the point dipole approximation applies, i.e., the unpaired electrons are located at the metal ion, the paramagnetic relaxation enhancement is given by (Solomon, 1955)

$$R_{1\mathrm{p}} = \frac{2}{15}\left(\frac{\mu_0}{4\pi}\right)^2 S(S+1) g_{\mathrm{e}}^2 \mu_{\mathrm{B}}^2 \gamma_I^2 r^{-6} \times \left[\frac{3\tau_{\mathrm{c},1}}{1+\omega_I^2\tau_{\mathrm{c},1}^2} + \frac{7\tau_{\mathrm{c},2}}{1+\omega_S^2\tau_{\mathrm{c},2}^2}\right]. \tag{2}$$

Here, ω_I and ω_S are the Larmor frequencies of the nuclear spin I and the electron spin S, respectively.

Further, γ_I is the gyromagnetic ratio of the nuclear spin I, g_e is the electron g-factor, S is the electron spin quantum number, μ_B is the Bohr magneton, and μ_0 is the permeability of free space. Finally, r is the distance between the metal ion and the nucleus. The correlation times, $\tau_{c,1}$ and $\tau_{c,2}$, can be written as

$$\tau_{c,1} = (\tau_r^{-1} + R_{1e})^{-1}, \quad (3)$$

$$\tau_{c,2} = (\tau_r^{-1} + R_{2e})^{-1}, \quad (4)$$

where R_{1e} and R_{2e} are the longitudinal and the transverse electron relaxation rates, respectively, while τ_r is the correlation time for the rotational reorientation of the complex. If chemical exchange is present in the protein and affects the nucleus-electron interaction, the rate of the exchange process must be included in Equations 3 and 4.

Materials and methods

Materials

Cloning, expression, and purification of the ^{15}N-labeled HHP–tagged *E. coli* Trx were performed by the research group at Unizyme Laboratories, as described below. Cysteamine-HCl, lysozyme and benzonase were obtained from Sigma. Sephadex G-25 F and Chelate-Sepharose FF were from Amersham Biosciences (Uppsala, Sweden). The ^{15}N enriched growth medium Celtone-N (>98% ^{15}N) was the product of Martek Biosciences Corp. (Columbia MD).

Strains and plasmids

E. coli strain TOP10 (Invitrogen) was used as host for DNA constructions and BL21 (Novagen) was used as host for protein production. The Trx encoding sequence of the vector pTrx (Invitrogen) was amplified by PCR using a forward primer [5′-AACATCATGAAACACCAACACCAACATCAACA TCAACATCATCCAAGCGATAAAATTATTCACCT GACT] introducing the polyhistidine tag encoding sequence (MK-(HQ)4-HHP) and a BspHI restriction site, and a reverse primer [5′-GCCGAATTCGGATCC TTACTAGGCCAGGTTAGCGTCG] introducing a BamHI restriction site downstream of the stop codon. The amplified 0.38-kb DNA fragment was digested by BspHI and BamHI and ligated into the NcoI and BamHI restriction sites of pTrcHisA (Invitrogen) resulting in the expression plasmid pCLU97-1.

Expression of MK-(HQ)4-HHP-Trx

BL21 harboring pCLU97-1 was used to produce MK-(HQ)4-HHP-Trx. Starter cultures were grown at 32°C in standard LB medium supplemented with ampicillin. 2 L shaker flasks with 5–600 mL Celtone-N medium supplemented with ampicillin were inoculated with starter culture (approx. 1:80) and were grown at 32 °C to mid-log phase and expression of recombinant protein was induced by adding isopropyl-1-thio-β-galactopyranoside (IPTG) to a final concentration of 0.06 mM. Cells were grown for an additional 20 h at 32 °C and harvested by centrifugation.

Purification of MK-(HQ)4-HHP-Trx

IMAC purification of MK-(HQ)4-HHP-Trx was performed essentially as described previously (Pedersen et al., 1999). The chromatographic purification steps were performed at 20–25 °C. Cells from approximately 2.5 liters of culture were harvested by centrifugation and resuspended in 120 mL buffer A (20 mM sodium phosphatebuffer, 300 mM NaCl, 20 mM imidazole, pH 7.5). Lysis was performed by a freeze/thaw cycle and subsequent treatment with lysozyme (0.75 mg/mL) and benzonase (50 units/mL) for 1 h at 4 °C. After centrifugation the supernatant was loaded at a flowrate of 5 mL/min onto a Ni^{2+} -Chelate-Sepharose FF column (5.3 cm^2 × 12 cm) equilibrated with buffer A and the column was washed with 125 mL buffer A. MK-(HQ)4-HHP-Trx was eluted by a linear gradient (225 mL) from buffer A to buffer B (20 mM sodium phosphatebuffer, 300 mM NaCl, 1 M imidazole, pH 7.5) at a flow rate of 2.5 mL/min. Fractions of 5 mL were collected and fractions (65 mL) containing MK-(HQ)4-HHP-Trx were identified by SDS-PAGE and pooled. The preparation was made 5 mM in EDTA and desalted on a Sephadex G-25 F column (5.3 cm^2 × 30 cm) equilibrated with 20 mM sodium phosphate, 150 mM NaCl, pH 7.0.

Preparation of HHP-Trx from MK-(HQ)4-HHP-Trx

HT-DPPI cleavage of the MK-(HQ)4-Tag was performed essentially as described previously (Pedersen et al., 1999). Preparative HT-DPPI cleavage of MK-(HQ)4-HHP-Trx (475 mg) was carried out in 20 mM sodium phosphate, 150 mM NaCl, pH 7.0 at a protein concentration of 3 mg/mL. HT-DPPI activated with 10 mM cysteamine for 5 min at 37 °C was added to the protein at a concentration of 75 munit per mg, and the mixtures were incubated at 37 °C for 60 min.

The progress of the cleavage reaction was followed by SDS-PAGE. After the enzymatic reaction, the mixture was desalted on a Sephadex G-25 F column (19.6 cm^2 × 27 cm) equilibrated with 20 mM sodium phosphate, 150 mM NaCl, 15 mM imidazole, pH 7.5. The desalted HHP-Trx was pumped through a Ni^{2+}-Chelate-Sepharose FF column (5.3 cm^2 × 12 cm) at a flowrate of 2 mL/min to remove uncleaved MK-(HQ)4-HHP-Trx and other protein contaminants. The flow-through containing HHP-Trx was finally desalted on a Sephadex G-25 F column (19.6 cm^2 × 54 cm) equilibrated with 10 mM sodium phosphate, pH 7.5. The yield of HHP-Trx was 350 mg corresponding to 140 mg/L of *E. coli* culture.

NMR samples

The uniformly ^{15}N-labeled HHP-Trx was dissolved in 90% H_2O/10% D_2O with 50 mM sodium chloride. The protein concentration was 1.0 mM in all samples. The pure oxidized form of HHP-Trx was obtained by adding 5 μL 50 mM H_2O_2 to each one of the NMR samples (500 μL). The pH was adjusted to 7.0 (meter reading) and the samples were sealed off under nitrogen, except for those used in the pH titration experiments. Coordination of the paramagnetic Ni^{2+} and the diamagnetic Zn^{2+} ions was achieved by adding the appropriate amounts of $NiCl_2 \cdot 6H_2O$ and $ZnCl_2$ to the protein samples.

NMR spectroscopy

The NMR experiments were carried out at 298 K and a ^1H frequency of 500 MHz using a Varian Inova 500 spectrometer. In all experiments, the ^1H carrier was placed on the HDO residual resonance located at 4.774 ppm at 298 K (Wishart and Sykes, 1994).

The longitudinal ^1H relaxation rates of the amide protons of the oxidized form of HHP-Trx were obtained by two-dimensional, inversion recovery (IR) ^1H-^{15}N HSQC experiments using 11 relaxation delays of 0.01, 0.02, 0.04, 0.08, 0.16, 0.32, 0.64, 1.2, 2.4, 4.8, and 8.0 s. The partly relaxed spectra were recorded in random order and a recurrent manner, as described previously (Ma et al., 2000), to eliminate systematic errors. The spectra were collected with either 2048 or 4096 t_2 data points and 150 t_1 slices, and with sweep widths of 10 kHz and 2 kHz in the ^1H and ^{15}N dimensions, respectively. The longitudinal relaxation rates were extracted from the spectra by an exponential three-parameter fit of the signal intensities versus the delay times.

The ^{15}N longitudinal and transverse relaxation rates were measured using the gradient sensitivity-enhanced pulse sequences (Farrow et al., 1994). The R_1 experiment was collected with 2048 t_2 data points, 160 t_1 slices, and 12 relaxation delays of 0.010, 0.020, 0.040, 0.080, 0.161, 0.322, 0.503, 0.704, 0.905, 1.207, 1.509, 1.911 s. The R_2 experiment was collected with 2048 t_2 data points, 200 t_1 slices, and ten relaxation delays of 0, 8, 16, 32, 48, 64, 96, 112, 128, and 144 ms. In both the R_1 and R_2 experiments, the sweep widths were 10 kHz and 2 kHz in the ^1H and ^{15}N dimensions, respectively. The ^{15}N R_1 and R_2 relaxation rates were extracted from the spectra by an exponential two-parameter fit of the signal intensities versus the delay times.

Results and discussion

Assignment of the HHP-Trx spectra at pH 7.0

The signals of the ^1H-^{15}N HSQC spectra of the oxidized, metal free HHP-Trx at pH 5.7 and 298 K were identified on the basis of the previous assignments of the ^1H and ^{15}N spectra of oxidized Trx at pH 5.7 and 308 K (Chandrasekhar et al., 1991). The assignment of the ^1H-^{15}N HSQC spectra of the metal coordinated HHP-Trx at pH 7.0 and 298 K was obtained from a pH titration of Zn^{2+}-HHP-Trx by following the variation of the spectra from pH 7.0 to 5.7 at 298 K.

Binding ability of the HHP-tag towards metal ions at pH 7.0

Initially, the metal binding ability of HHP-Trx towards the diamagnetic Zn^{2+} ion was investigated. Thus, the overall rotational correlation time, τ_r, of HHP-Trx in the presence of an equivalent amount of Zn^{2+} was compared with τ_r of the metal free HHP-Trx. The correlation times were determined from the ratio of the R_1 and R_2 relaxation rates of the protein backbone ^{15}N nuclei (Kay et al., 1989). The correlation time was 8.76 ns for the Zn^{2+} complex and 6.16 ns for the metal free HHP-Trx in 1.0 mM protein solutions at pH 7.0 and 298 K. The latter correlation time is in good agreement with the value of 6.41 ns obtained previously for the oxidized form of Trx at pH 5.7 and 308 K (Stone et al., 1993). The difference in correlation times between the free and the metal complex of HHP-Trx clearly suggests that more than one protein molecule is bound to each Zn^{2+} ion.

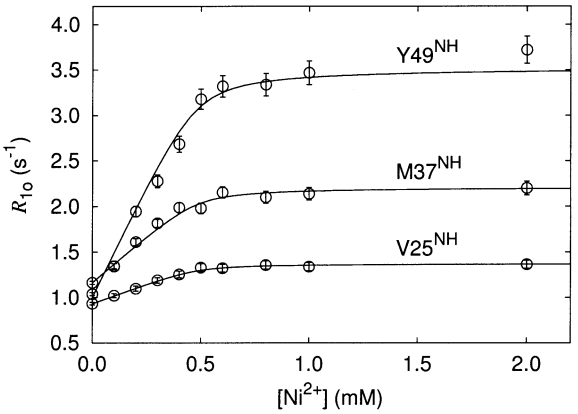

Figure 1. The observed longitudinal relaxation rates, R_{1o}, of the amide protons $V25^{NH}$, $M37^{NH}$, and $Y49^{NH}$ in HHP-Trx in a series of 1.0 mM protein samples with increasing Ni^{2+} concentrations. The samples were dissolved in 90% H_2O/10% D_2O with 50 mM sodium chloride at pH 7.0 (meter reading). The constant relaxation rates observed at Ni^{2+} concentrations above 0.5 mM, indicate the formation of the dimer complex, $Ni(HHP\text{-}Trx)_2^{2+}$. The curves correspond to the binding constants $K_1 = K_2 = 20\ mM^{-1}$ of the successive binding of the two HHP-Trx molecules (see text).

A similar investigation of the binding ability towards Ni^{2+} is prevented by the paramagnetic contribution to the ^{15}N relaxation rates. Instead, the number of ligands bound to the Ni^{2+} ion, and the stability of the Ni^{2+}-HHP-Trx complex were investigated by measuring the dependence of the longitudinal relaxation rates of the amide protons on the Ni^{2+} concentration. Ten 1.0 mM HHP-Trx samples with different Ni^{2+} concentrations (0.0, 0.1, 0.2, 0.3, 0.4, 0.5, 0.6, 0.8, 1.0, and 2.0 mM) were used. Figure 1 shows the variation of the observed relaxation rates, R_{1o}, with increasing Ni^{2+} concentration for three different amide protons. As shown in the figure, the relaxation rates increase linearly until a $[Ni^{2+}]$/[HHP-Trx] ratio of 0.5. However, above this ratio the rates remain approximately constant up till the highest Ni^{2+} concentration applied, that is $[Ni^{2+}] = 2.0$ mM corresponding to a $[Ni^{2+}]$/[HHP-Trx] ratio of 2. This relaxation profile, which applies to a substantial part of the amide protons in HHP-Trx, shows that each Ni^{2+} ion binds two protein molecules. In addition, the constant values of the relaxation rates for $[Ni^{2+}]$/[HHP-Trx] > 0.5 exclude the presence of other strong metal binding sites in the protein at the applied pH of 7.0. For $[Ni^{2+}]$/[HHP-Trx] < 0.5 the dependence of the observed relaxation rates, R_{1o}, on the Ni^{2+} concentration is given by

$$R_{1o} = R_1^{dia} + \frac{2\left[Ni^{2+}\right]}{[\text{HHP-Trx}]} R_{1p}. \quad (5)$$

This dependence, together with the fact that exchange-averaged signals are observed for nearly all the amide protons in the metal bound HHP-Trx (see below), show that the fast exchange condition applies (McLaughlin and Leigh, 1973). It should be noted that the exchange-averaged signals are compatible with different binding geometries for the two protein ligands in the 1:2 complex.

The successive binding of the two protein ligands (P) can be described by the following equilibria

$$2P + Ni^{2+} \overset{K_1}{\rightleftharpoons} P + P - Ni^{2+} \overset{K_2}{\rightleftharpoons} P_2 - Ni^{2+}. \quad (6)$$

The data in Figure 1 do not allow a precise determination of the binding constants, K_1 and K_2, however, lower limits of the two constants can be obtained. Thus, the linear increase in the relaxation rates with increasing Ni^{2+} concentration up till $[Ni^{2+}]$/[HHP-Trx] $= 0.5$, and the abrupt change to a constant relaxation rate above this ratio, are only compatible with relatively large values for both binding constants. Therefore, the smallest values of the two binding constants that describe the variation of the relaxation rates in Figure 1 are $K_1 = K_2 = 20\ mM^{-1}$, assuming the absence of co-operative effects (i.e., $K_1 \geq K_2$), and ignoring a possible change in the rotational correlation time with increasing Ni^{2+} concentration. These values give an overall binding constant of $K = K_1 \times K_2 = 400\ mM^{-2}$. Other values of the two individual binding constants, which correspond to the same or a larger overall constant, are also in agreement with the experimental relaxation data. Still, the data in Figure 1 suggest that HHP-Trx forms a well-defined dimer complex with Ni^{2+}.

Additional metal binding sites in HHP-Trx

Unlike the dependences in Figure 1, the relaxation rates of a series of other amide protons continue to increase above the $[Ni^{2+}]$/[HHP-Trx] ratio of 0.5. This is illustrated in Figure 2 by the variation of the relaxation rates of the D20 amide proton with the Ni^{2+} concentration. Since the HHP-tag is unable to bind additional Ni^{2+} ions above the $[Ni^{2+}]$/[HHP-Trx] ratio of 0.5, the increase of the relaxation rates in Figure 2 for $[Ni^{2+}] > 0.5$ mM reveals the presence of an additional Ni^{2+} binding site in the protein. Similar relaxation increases were observed for other amide protons, in particular the amide protons of residues in the regions from T8 to G21, from K82 to T89, and from E101 to A108. Therefore, several additional metal binding sites are available in the protein.

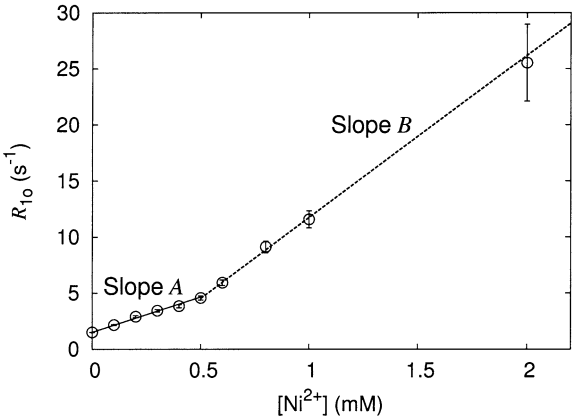

Figure 2. The observed longitudinal relaxation rates, R_{1o}, of the amide proton $D20^{NH}$ in HHP-Trx in a series of 1.0 mM protein samples with increasing Ni^{2+} concentrations. The experimental conditions were as in Figure 1. The solid line corresponds to a linear least squares fit of the relaxation rates in the Ni^{2+} concentration range from 0.0 mM to 0.5 mM (slope A), while the dashed line corresponds to a similar fit of the rates in the Ni^{2+} concentration range from 0.5 mM to 2.0 mM (slope B). The increase of the relaxation rates with increasing Ni^{2+} concentration above 0.5 mM indicates the presence of an additional binding site in the protein.

Yet, the Ni^{2+} binding ability of these sites is relatively weak since only amide protons spatially close to the binding sites are affected. This is illustrated in Figure 3, where the additional relaxation is quantified by the ratio B/A, A and B being the slopes of the relaxation increase below and above the [Ni^{2+}]/[HHP-Trx] ratio of 0.5, respectively (see Figure 2). Thus, a large B/A ratio shows that the contribution from the Ni^{2+} ion in an additional binding site is significant, while a B slope close to zero shows that the amide proton is only little affected or unaffected by the additional Ni^{2+} binding. Figure 3 shows that the ratio B/A has several local maxima along the sequence, and that the maxima in most cases are defined by several experimental ratios. Most importantly, however, Figure 3 shows that all the maxima are located in regions with residues that have a side chain carboxylate group, that is aspartic acid and glutamic acid residues. Thus, the results in Figure 3 indicate that Ni^{2+} binds to the side chain carboxylate groups of the Asp and Glu residues in HHP-Trx. The specific Asp and Glu residues that are located in the maxima regions are indicated in Figure 3. Similar observations were previously made for the interaction between the carboxylate groups of the protein calbindin and the paramagnetic gadolinium complex Gd-DO3A (Aime et al., 2002).

This conclusion is further supported by the shoulder on the E85 maximum in Figure 3. Thus, the side chain carboxylate group of D20 is spatially close to the amide protons of the residues N83 and G84. Residues that belong to the local maximum around E85 are therefore affected also by the Ni^{2+} ion bound to the carboxylate group of D20. Similarly, the Ni^{2+} ion bound to the side chain carboxylate group of D9 enhances the relaxation rates of the amide protons in the residues N63 and G65.

The amide proton signals of a number of residues were missing or weak at the applied conditions and were, therefore, not included in the analysis. These are the amide proton signals from the two tag-histidines, H-2 and H-1, and from $S1^{NH}$, $D2^{NH}$, $K3^{NH}$, $I4^{NH}$, $T77^{NH}$, and $S95^{NH}$. Also, the signal from $G33^{NH}$ was visible only at pH values lower than 6.0, while the signals from the residues C32, G51, R73, G74, K96, and G97 were excluded since a correct estimation of their relaxation rates was obscured by a none-single exponential relaxation behavior.

Finally, the relaxation of the amide protons in the region from L42 to D48 does not follow the behavior shown in Figure 1 or Figure 2. The amide protons of D43 and E44 are broadened beyond detection at Ni^{2+} concentrations larger than 0.4 mM. Furthermore, the amide proton signals of L42, I45, A46, D47, and E48 show characteristics indicating that these protons are in the slow exchange regime or close to this regime. Thus, in the diamagnetic sample only one signal is present for each of these amide protons, while a second signal appears as the concentration of the Ni^{2+} ions is increased. At even larger Ni^{2+} concentrations only the second signal is visible. Moreover, the second signal relaxes considerably faster than the first one. These observations indicate that the two signals correspond to a free and a metal bound form of the protein, respectively. It is suggested that two or more of the spatially close side chain carboxylate groups of D43, E44, D47, and E48 bind the paramagnetic Ni^{2+} ion leaving the L42, I45, A46, D47, and E48 amide protons in or close to the slow exchange regime.

The pH dependence of the metal binding ability of the HHP-tag

The pH dependence of the binding ability of HHP-Trx towards Ni^{2+} was investigated in the pH range from 3.5 to 7.5, using a 1.0 mM solution of HHP-Trx with an equivalent amount of Ni^{2+}. An IR ^{1}H-^{15}N HSQC experiment was recorded for each step of the titration. Figure 4 shows the observed longitudinal relaxation rates, R_{1o}, of the amide proton $A56^{HN}$ versus pH. At

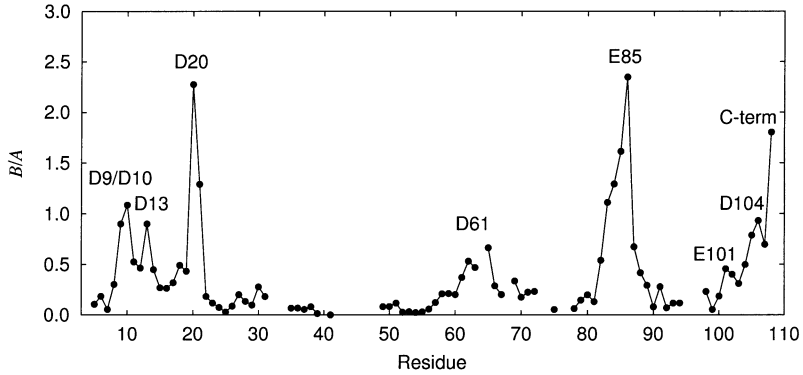

Figure 3. A plot of the ratio B/A as a function of the residue number. A and B are the slopes defined in Figure 2 and describe the variation of the relaxation rates with increasing Ni^{2+} concentration in the range from 0.0 mM to 0.5 mM, and from 0.5 mM to 2.0 mM, respectively. A large B/A ratio indicates that the amide proton is strongly affected by Ni^{2+} bound to other metal binding sites in the protein than the HHP-tag. A ratio close to zero indicates that the amide proton is unaffected by these sites. The largest B/A ratios are obtained for the amide protons of residues with side chain carboxylate groups (aspartic and glutamic acids) or residues close to these groups, indicating that the side chain carboxylate groups are additional metal binding sites.

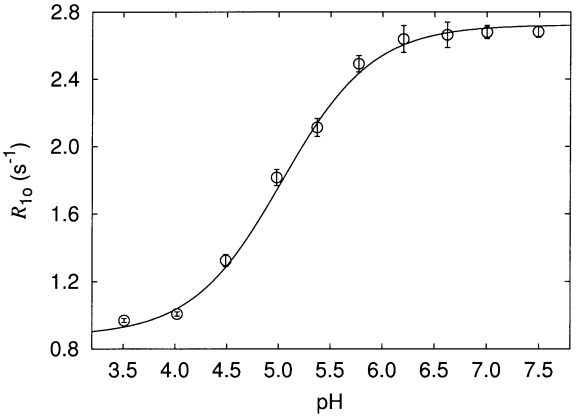

Figure 4. The pH dependence of the observed longitudinal relaxation rates, R_{1o}, of the amide proton $A56^{NH}$ in HHP-Trx obtained from a 1.0 mM solution of the protein containing an equivalent amount of Ni^{2+}. The titration curve is a least squares fit corresponding to an effective one-step titration ($pK_a = 5.04 \pm 0.06$).

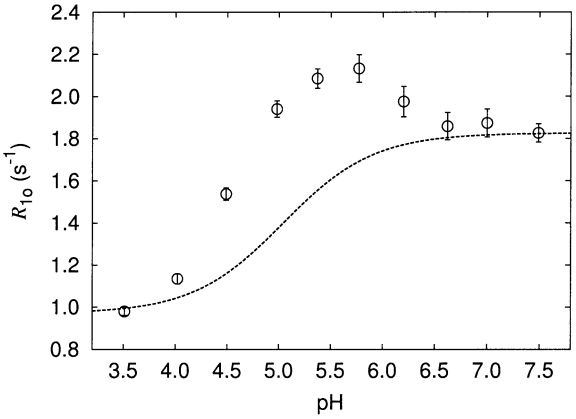

Figure 5. The pH dependence of the observed longitudinal relaxation rates, R_{1o}, of the amide proton $D13^{NH}$ in HHP-Trx obtained from a 1.0 mM solution of the protein containing an equivalent amount of Ni^{2+}. The dashed line is the titration curve corresponding to a pK_a value of 5.04 (see Figure 4). The deviations of the R_{1o} rates from the titration curve are caused by the binding of Ni^{2+} to the side chain carboxylate group of D13.

pH 3.5 the R_{1o} rate is identical to that observed in the free HHP-Trx protein, indicating that the paramagnetic Ni^{2+} ion does not bind to the protein at this pH. In contrast, around pH 7 R_{1o} reaches a maximum rate that is approximately 3 times faster than the rate of the metal free protein. This increase corresponds to a substantial paramagnetic contribution to the relaxation rate, and shows that Ni^{2+} binds to the HHP-Trx protein. An effective pK_a of 5.04 ± 0.06 was obtained from the titration data, in agreement with the pK_a value expected for a histidine imidazole ring (Kojiro and Markley, 1983). This clearly indicates that the Ni^{2+} ion competes with the H^+ ion for the binding to the imidazole rings of the histidine residues, more specifically to the δ nitrogens of the rings.

However, the pH titration of several other amide protons is atypical, with a maximum on the titration curves between pH 5.4 and pH 5.8. This is illustrated in Figure 5 for the amide proton $D13^{NH}$. In general, this pH dependence was observed for the same amide protons for which the relaxation rates increase in the Ni^{2+} concentration range where $[Ni^{2+}]/[\text{HHP-Trx}] > 0.5$ (T8-G21, K82-T89, E101-A108, see Figure 2). Therefore, the atypical increase of R_{1o} in the pH range from 5.4 to 5.8 is most likely caused by the additional

binding of paramagnetic Ni^{2+} ions to the side chain carboxylate groups, discussed above. Admittedly, the atypical increases could also be caused by pH-induced structural changes of the protein. However, previous studies of the pH dependence of the ^1H chemical shifts of both reduced and oxidized Trx indicate that the structure, in general, remains unchanged between pH 5.7 and pH 10 (Dyson et al., 1991). Therefore, it is unlikely that structural changes are responsible for the observed R_{1o} maxima in the pH range from 5.4 to 5.8.

On the other hand, the relaxation maxima are in good agreement with the binding of Ni^{2+} to the side chain carboxylate groups. Thus, pK_a values of the side chain carboxylic acids, that are smaller than the effective pK_a value of the histidine imidazole rings of the HHP-tag, will favor metal binding to the carboxylate groups at lower pH values. More precisely, when the pH is lowered and approaches the pK_a value of the HHP-tag, the Ni^{2+} ions will still have full access to the side chain carboxylate groups but will meet increasing competition from H^+ ions for the imidazole groups of the HHP-tag. Consequently, more Ni^{2+} ions will be available for binding to the carboxylate groups when the pH is lowered. In agreement with this scenario, the pK_a values of the side chain acid groups in the seven residues, D9, D10, D13, D15, D20, E101, and D104, are in the range from 3.8 (D104) to 4.9 (D9), according to the pH dependence of the chemical shifts of the amide protons and the backbone ^{15}N nuclei of HHP-Trx. The corresponding pK_a value of the glutamic acid E85 could not be obtained due to spectral overlap. As discussed above on the basis of the local paramagnetic relaxation effects (Figure 3), the metal binding constants of the side chain groups are small compared to that of the HHP-tag, allowing only a minor fraction of the metal ions to be bound to the side chain groups. Here, this is reflected by the moderate relaxation increase in Figure 5. At low pH values (pH $\approx$ 3.5), protonation of the side chain acid groups prevents a binding of metal ions also to these groups.

Long-range structure information from the HHP-bound Ni^{2+}

The solution structure of the oxidized form of Trx was solved previously by NMR using the programs DYANA and AMBER (Jeng et al., 1994). The obtained structure is well-defined with a root mean square deviation (RMSD) of 0.35 Å for the backbone (residues 4-107) within an ensemble of 20 structures.

Here the structure of the dimer complex of HHP-Trx with Ni^{2+} was calculated from the same NOE and dihedral angle constraints as used in the previous calculation of the monomer structure (Jeng et al., 1994), using the program XPLOR (Brünger, 1992). Initially, the structure was calculated without inclusion of the paramagnetic distance constraints. The two monomers were bound to the metal ion through bonds from the histidine N^{δ} atoms of the HHP-tag (bond length 2.09 Å). A total of 60 structures were calculated as described previously (Ma et al., 2000). In all calculations, the force constants used for the NOE and the dihedral angle constraints were 50 kcal·mol^{-1}·Å^{-2} and 200 kcal·mol^{-1}·rad^{-2}, respectively. The backbone RMSD of each of the two monomer subunits was 0.29 Å (residues 4-107), while the structure around the metal binding tag was poorly defined since no NOE or dihedral angle constraints were obtained for the tag-residues.

Subsequently, a structural refinement was performed, now with the paramagnetic distance constraints included. Only amide protons with the relaxation profile shown in Figure 1, that is, amide protons which are unaffected by the carboxylate binding sites in the protein, were included in the structure calculation. In practice, only amide protons with resolved signals in the HSQC spectra that fulfill the inequality $B/A \leq 0.20$ were included. Using this criteria, a total of 26 amide protons were accepted. The paramagnetic relaxation enhancements of these amide protons were derived from the rates obtained in the Ni^{2+} titration experiments using Equation **??**, and converted into distances by applying Equation 2 and the electron relaxation rates $R_{1e} = (7.6 \pm 0.9)\times10^9$ s^{-1} and $R_{2e} = (9.4 \pm 1.5)\times10^9$ s^{-1} (Jensen and Led, 2004). The experimental uncertainties of both the R_{1p} rates and the electron relaxation rates were taken into account when calculating the uncertainty of the paramagnetic distance constraints.

The paramagnetic constraints were included in the XPLOR structure calculations using the NOE square-well energy function. In this structure calculation, the two monomers were regarded as rigid bodies in the range from I4 to A108, that is, only translation and rotation of the two monomers were allowed. The Ni^{2+} ion, the tag, and the residues from S1 to K3 were all allowed to move freely, only restrained by the Ni^{2+}-histidine bonds and the topology of the individual amino acids.

Initially, it was assumed that the dimer complex is symmetric. Therefore, a separate set of paramagnetic

distances was included for each of the two monomers, that is, a total of 52 paramagnetic distances were applied, 26 identical constraints for each monomer. Figure 6 shows a comparison of the distances r_{para} and r_{struct} obtained in this structural refinement. Here, r_{para} are the distances derived from the R_{1p} rates using Equation 2, while r_{struct} are the corresponding distances obtained from the lowest energy structure of the symmetric Ni^{2+} dimer complex of HHP-Trx. The solid line in the figure corresponds to the ideal case where $r_{struct} = r_{para}$. Clearly, the agreement between the two sets of distances is poor, and the deviations from the ideal case are far beyond the experimental errors. Therefore, the assumption of a symmetric dimer complex does not apply.

A new refinement of the structure was performed assuming an asymmetric dimer complex. Since only a single paramagnetic distance is available for each of the 26 amide protons, the distances were averaged according to the equation

$$\langle r_{struct}^{-6} \rangle^{-1/6} = \left[\frac{1}{2} \left(r_1^{-6} + r_2^{-6} \right) \right]^{-1/6}. \qquad (7)$$

Here, r_1 and r_2 are the metal-nucleus distances in the two monomers, respectively. During the structural refinement the difference between $\langle r_{struct}^{-6} \rangle^{-1/6}$ and r_{para} was minimized by varying the orientation of the two monomers relative to the Ni^{2+} ion. Figure 7 compares the r_{para} and the $\langle r_{struct}^{-6} \rangle^{-1/6}$ distances in the lowest energy structure of the asymmetric dimer complex thus obtained. The discrepancies in Figure 6 have now disappeared and only small deviations (< 0.5 Å) from the ideal case are observed. Even though the number of parameters to be fit is increased when going from the symmetric to the asymmetric model, the system is still considerably overdetermined. Thus, the fit in Figure 7 clearly indicates that the dimer complex is in fact asymmetric. Moreover, it shows that the paramagnetic constraints are in good agreement with the NOE structure of the protein. Finally, the agreement between the NOE structure and the paramagnetic constraints shows that the metal binding tag does not affect the structure of the protein significantly. A ribbon model of the lowest energy structure of the asymmetric dimer complex is shown in Figure 8. The green sphere indicates the paramagnetic Ni^{2+} ion.

It should be noted that although the paramagnetic distance constraints orient the two monomers relative to the Ni^{2+} ion, the orientation of the two monomers relative to each other remains somewhat undetermined, mainly because the fast ligand exchange prevents the observation of inter-monomer constraints. In agreement with this, the structures of the two monomer subunits cannot be superimposed at the same time.

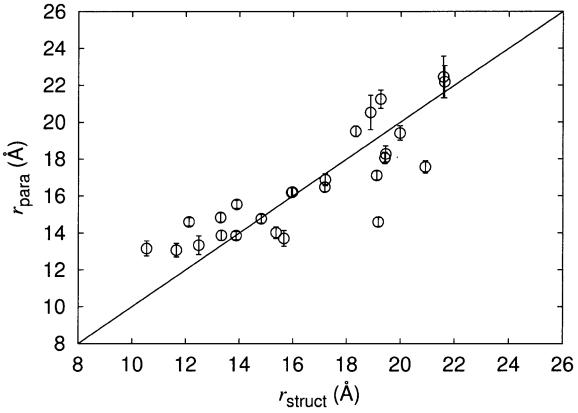

Figure 6. Comparison of the distances r_{para} and r_{struct} assuming a symmetric dimer complex. Here, r_{para} are the distances between the Ni^{2+} ion and the amide protons calculated from the paramagnetic relaxation enhancements at 11.74 T using Equation 2, while r_{struct} are the corresponding distances in the refined structure of the Ni^{2+}-HHP-Trx dimer complex with the lowest energy. Only the relaxation of resolved amide protons signals with $B/A \leq 0.2$ were included in the structural refinement. The solid line corresponds to the ideal case where $r_{para} = r_{struct}$.

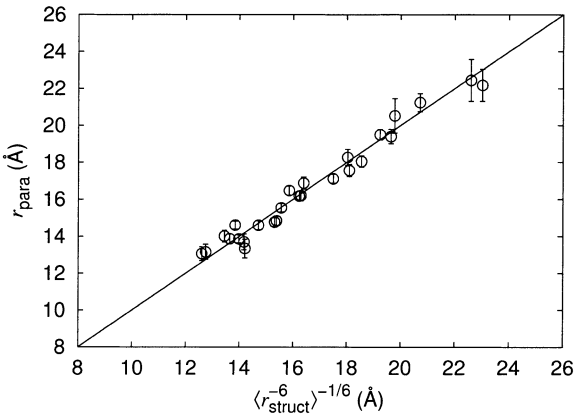

Figure 7. Comparison of the distances r_{para} and $\langle r_{struct}^{-6} \rangle^{-1/6}$ assuming an asymmetric dimer complex. Here, r_{para} are the distances between the Ni^{2+} ion and the amide protons calculated from the paramagnetic relaxation enhancements at 11.74 T using Equation 2, while $\langle r_{struct}^{-6} \rangle^{-1/6}$ corresponds to the r^{-6} average of the two individual monomer distances, given by Equation 7. Only the relaxation of resolved amide protons signals with $B/A \leq 0.2$ were included in the structural refinement. The solid line corresponds to the ideal case where $r_{para} = \langle r_{struct}^{-6} \rangle^{-1/6}$.

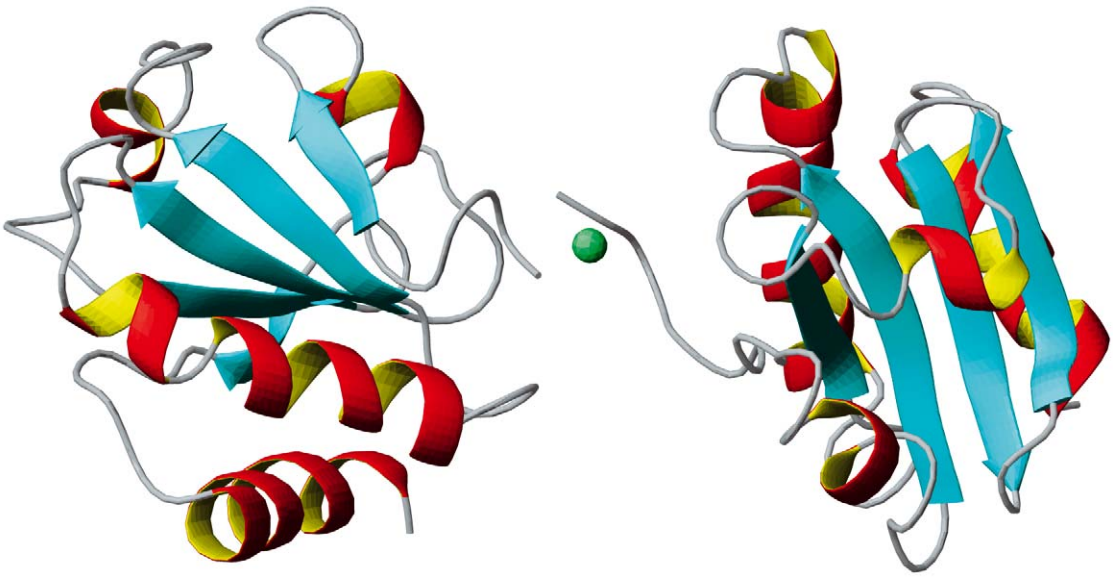

Figure 8. Ribbon model of the lowest energy structure of the asymmetric Ni^{2+} dimer complex of HHP-Trx. The green sphere indicates the Ni^{2+} ion. The figure was prepared using MOLMOL (Koradi et al., 1996).

Conclusion

In conclusion, the study shows that detailed information about the interaction of Ni^{2+} with a HHP-tagged protein can be obtained from the paramagnetic relaxation enhancements of the amide protons. Thus, the dependence of the amide proton relaxation rates on the Ni^{2+} concentration shows not only that each Ni^{2+} ion binds two protein molecules. It also reveals the presence and the location of a series of additional metal binding sites in the protein. These sites were identified as side chain carboxylate groups of Asp and Glu residues.

Furthermore, the pH titration of a sample of HHP-tagged thioredoxin containing an equivalent amount of Ni^{2+} shows that the Ni^{2+} ions bind to the HHP-tag only at neutral and high pH, where the histidine imidazole rings are deprotonated. Also, the pH dependence of the amide proton relaxation rates confirms the presence of the additional side chain carboxylate binding sites, and shows that the Ni^{2+} ions bind to these sites primarily in the pH range from 5.0 to 6.0, where the competition from the HHP-binding site is low or negligible.

Finally, the study shows that, in general, the competition from the additional metal binding sites must be taken into account, in order to obtain long-range distance constraints from the paramagnetic relaxation enhancements. However, the relaxation enhancements of a series of amide protons, which are unaffected by the side chain carboxylate binding sites, provide long-range distances that are consistent with the solution structure of thioredoxin. Moreover, these distances show that the structure of the protein is unaffected by the HHP-tag and reveal that the dimer complex is asymmetric.

Acknowledgements

We thank D. Flemming Hansen, Mathias A. S. Hass, Søren M. Kristensen, Berit I. Kristensen, and Kim Hejnæs for helpful discussions, and Else Philipp, Jens Duus, and Bent O. Petersen for technical assistance. We are grateful to H. Jane Dyson for providing the NOE and torsion angle constraints of thioredoxin. M.R.J. thanks Novo Nordisk A/S and Novozymes A/S for a scholarship. This work was financially supported by the Danish Natural Science Research Council (J. No.'s 9400351, 9801801, 51-00211 and 21-01-0545), Direktør Ib Henriksens Fond, Carlsbergfondet and Novo Nordisk Fonden.

References

Aime, S., D'Amelio, N., Fragai, M., Lee, Y.-M., Luchinat, C., Terreno, E. and Valensin, G. (2002) *J. Biol. Inorg. Chem.*, **7**, 617–622.

Bertini, I., Couture, M.M.J., Donaire, A., Eltis, L.D., Felli, I.C., Luchinat, C., Piccioli, M. and Rosato, A. (1996) *Eur. J. Biochem.*, **241**, 440–452.
Brünger, A.T. (1992) *XPLOR – A System for X-Ray Crystallography and NMR, Version 3.1.*, Yale University Press, New Haven.
Chandrasekhar, K., Krause, G., Holmgren, A. and Dyson, H.J. (1991) *FEBS Lett.*, **284**, 178–183.
Donaldson, L.W., Skrynnikov, N.R., Choy, W.-Y., Muhandiram, D.R., Sarkar, B., Forman-Kay, J.D. and Kay, L.E. (2001) *J. Am. Chem. Soc.*, **123**, 9843–9847.
Dyson, H.J., Gippert, G.P., Case, D.A., Holmgren, A. and Wright, P.E. (1990) *Biochemistry*, **29**, 4129–4136.
Dyson, H.J., Tennant, L.L. and Holmgren, A. (1991) *Biochemistry*, **30**, 4262–4268.
Farrow, N.A., Muhandiram, R., Singer, A.U., Pascal, S.M., Kay, C.M., Gish, G., Shoelson, S.E., Pawson, T., Forman-Kay, J.D. and Kay, L.E. (1994) *Biochemistry*, **33**, 5984–6003.
Gaponenko, V., Altieri, A.S., Li, J. and Byrd, R.A. (2002) *J. Biomol. NMR*, **24**, 143–148.
Gaponenko, V., Dvoretsky, A., Walsby, C., Hoffman, B.M. and Rosevear, P.R. (2000) *Biochemistry*, **39**, 15217–15224.
Gochin, M. (2000) *Structure*, **8**, 441–452.
Gueron, M. (1975) *J. Magn. Reson.*, **19**, 58–66.
Holmgren, A. (1985) *Annu. Rev. Biochem.*, **54**, 237–271.
Jeng, M.-F., Campbell, A.P., Begley, T., Holmgren, A., Case, D.A., Wright, P.E. and Dyson, H.J. (1994) *Structure*, **2**, 853–868.
Jensen, M.R. and Led, J.J. (2004) *J. Magn. Reson.*, **167**, 169–177.
Kay, L.E., Torchia, D.A. and Bax, A. (1989) *Biochemistry*, **28**, 8972–8979.
Kojiro, C.L. and Markley, J.L. (1983) *FEBS Lett.*, **162**, 52–56.
Koradi, R., Billeter, M. and Wüthrich, K. (1996) *J. Mol. Graphics*, **14**, 51–55.
Ma, L., Jørgensen, A.-M.M., Sørensen, G.O., Ulstrup, J. and Led, J.J. (2000) *J. Am. Chem. Soc.*, **122**, 9473–9485.
Mal, T.K., Ikura, M. and Kay, L.E. (2002) *J. Am. Chem. Soc.*, **124**, 14002–14003.
McLaughlin, A.C. and Leigh, J.S. (1973) *J. Magn. Reson.*, **9**, 296–304.
Pedersen, J., Lauritzen, C., Madsen, M.T. and Dahl, S.W. (1999) *Protein Express. Purif.*, **15**, 389–400.
Solomon, I. (1955) *Phys. Rev.*, **99**, 559–565.
Stone, M.J., Chandrasekhar, K., Holmgren, A., Wright, P.E. and Dyson, H.J. (1993) *Biochemistry*, **32**, 426–435.
Tjandra, N. and Bax, A. (1997) *Science*, **278**, 1111–1114.
Tjandra, N., Omichinski, J.G., Gronenborn, A.M., Clore, G.M. and Bax, A. (1997) *Nat. Struct. Biol.*, **4**, 732–738.
Tolman, J.R., Flanagan, J.M., Kennedy, M.A. and Prestegard, J.H. (1995) *Proc. Natl. Acad. Sci. USA*, **92**, 9279–9283.
Tu, K. and Gochin, M. (1999) *J. Am. Chem. Soc.*, **121**, 9276–9285.
Vega, A.J. and Fiat, D. (1976) *Mol. Phys.*, **31**, 347–355.
Wishart, D.S. and Sykes, B.D. (1994) *Meth. Enzymol.*, **239**, 363–392.
Wüthrich, K. (1986) *NMR of Proteins and Nucleic Acids*, John Wiley & Sons, New York.
Wüthrich, K. (1994) *Curr. Opin. Struct. Biol.*, **4**, 93–99.